THE IMPORTANCE OF BOW SHOCK ADAPTION IN CFD SIMULATIONS FOR HYPERSONIC FLOWS

Jan B. Vos and Dominique Charbonnier

CFS Engineering, EPFL Innovation Park, Batiment A, 1015 Lausanne, Switzerland
jan.vos@cfse.ch, dominique.charbonnier@cfse.ch

ABSTRACT

Today design of re-entry flight vehicles relies heavily on numerical simulation of the aerodynamics and aero-thermodynamics phenomena involved, in particular in the hypersonic flight regime. It is well known that having a good quality grid is important to correctly predict heat fluxes on re-entry vehicles, in particular for capsule type of geometries. A recent development of the Navier Stokes Multi Block (NSMB) solver was the implementation of an automatic bow shock adaption procedure. During the calculation NSMB monitors the position of the bow shock wave, and once the bow shock does not move anymore NSMB will move the far field boundary towards this position and clusters grid points in this region. The use of the automatic bow shock adaption removes the tedious effort to align the grid to the bow shock for each flow condition to be simulated. As a result, only one grid is needed for the whole hypersonic/supersonic range, while at the same time the solution quality is improved, in particular for the heat fluxes.

Index Terms— Computational Fluid Dynamics, Shock adaption

1. INTRODUCTION

Hypersonic aerodynamics and aero-thermodynamics are concerned with the high-speed regime of a re-entry flight where certain physical phenomena, as dissociation and/or ionization of air or radiative heat transfer are important. These processes, which are absent in subsonic and supersonic flows, are triggered by the strong shock waves present around vehicles flying at hypersonic speeds. As a result, the characteristics of the flow and the aerodynamic loading and aero-thermodynamic heating on the re-entry vehicle are altered.

No ground facilities exist that are able to reproduce simultaneously all the physical phenomena of a re-entry flight vehicle. The American Space Shuttle was designed and developed in the 1970's using ground facilities together with approximate methods since the use of numerical methods was at that time still very limited. Although the first flight of the Space Shuttle was successful, several problems were encountered, the most serious one a much larger pitching moment than expected from design. The origin of this was later connected to the fact that in ground facilities it was not possible to simulate at the same time the high Mach number together with the dissociating air [1].

Since the design of the American Space Shuttle numerical simulation tools have undergone an impressive development while at the same time huge and cheap amounts of computer power have become available. Today design of re-entry flight vehicles rely heavily on numerical simulation of the aerodynamics and aero-thermodynamics phenomena involved, in particular in the hypersonic flight regime, while ground facilities are used for design verification and for CFD code validation.

The NSMB (Navier Stokes Multi Block) CFD code has its origins in the days of the Hermes Space Shuttle program [2]. The code was from the start of its development designed to be used for hypersonic re-entry flow simulations, and includes different levels of chemistry models up to electronic non-equilibrium. A recent development was the implementation of an automatic procedure to adapt the grid to the bow shock wave. During the calculation NSMB monitors the position of the bow shock wave, and once the bow shock does not move anymore NSMB will move the far field boundary towards this position and clusters grid points in this region.

Precise capturing of the bow shock wave [3] (or using a shock-fitting procedure) is required to:

- avoid the potential problem of the carbuncle near the stagnation line caused by the numerical dissipation of the space discretization scheme;
- avoid oscillations of flow quantities in the symmetry plane;
- avoid irregular heat fluxes (local extrema outside the symmetry plane, wavy behavior, iso-lines not normal to the symmetry plane). This is in particular important for capsule type of geometries where a large subsonic flow region exists on the heat shield just downstream of a strong bow shock wave, see the example shown in Figure 1.

In the past it was a tedious effort to generate the grid such that the grid is aligned with the bow shock, and this had to be

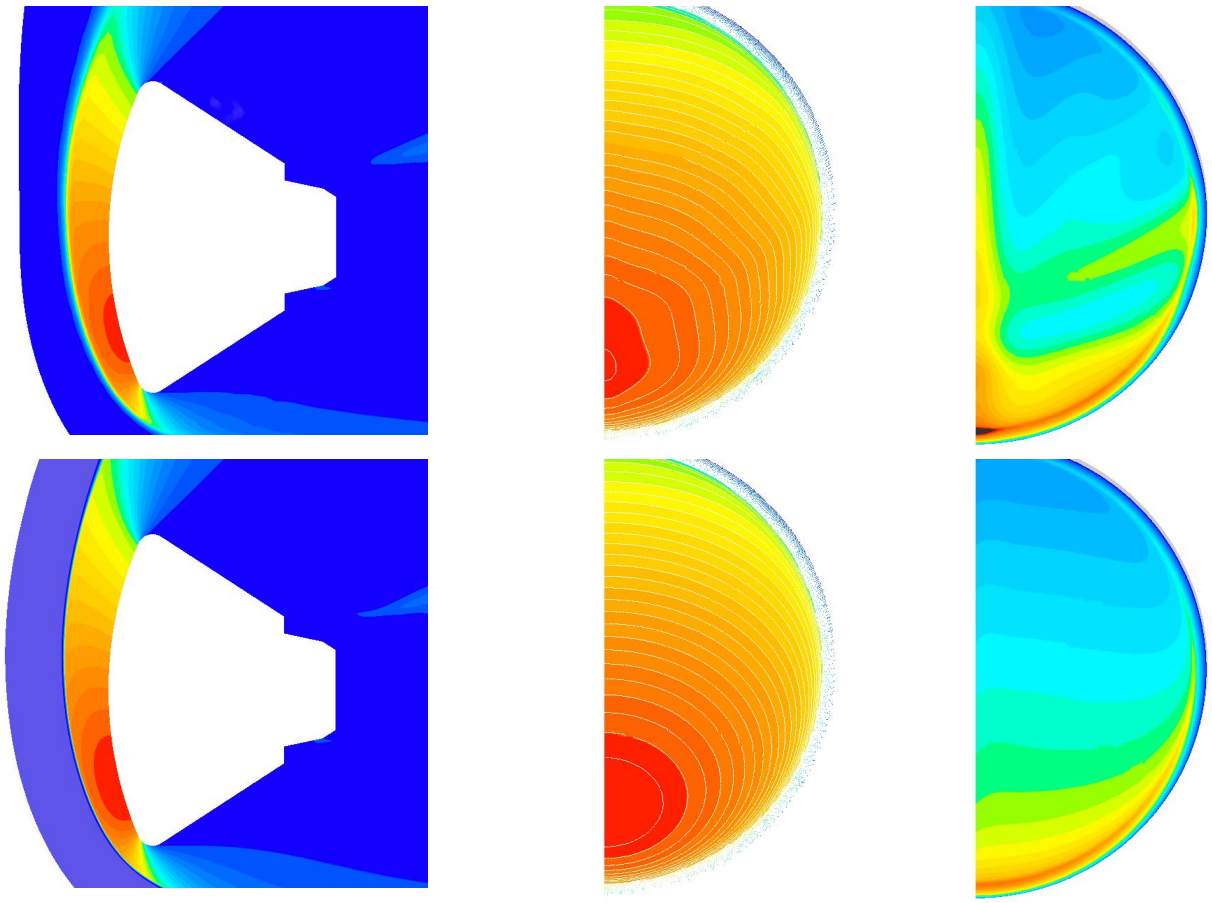

Figure 1: Use of grid adaption on a capsule type of geometry (ARD), top: non-adapted grid, bottom: adapted grid.

repeated for each flow condition. A first calculation was made (but not until convergence), the shock surface was extracted from the solution and imported in the mesh generator so that the grid could be adapted and clustered around the grid. This procedure had to be repeated several times until the shock did not move anymore. The use of the automatic bow shock adaption removes this effort since the solver adapts the grid to the bow shock position. As a result, only one grid is needed for the whole hypersonic/supersonic range, while at the same time the solution quality is improved, in particular the heat fluxes. Section 2 provides a short summary of the NSMB CFD solver, while Section 3 discusses the automatic shock adaption procedure. Results of calculations are presented in Section 4.

2. THE NSMB CFD SOLVER

The Navier Stokes Multi Block solver NSMB was initially developed in 1992 at the Swiss Federal Institute of Technology (EPFL) in Lausanne, and from 1993 onwards in the NSMB consortium composed of different universities, research establishments and industries. Today NSMB is developed by IMF-Toulouse (IMF Toulouse, France), ICUBE (Strasbourg, France), University of München (TUM, Germany), University of the Army in München (Germany), Airbus Safran (France), RUAG Aviation and CFS Engineering.

NSMB is a parallelized CFD solver employing the cell-centered finite volume method using multi block structured grids to discretize the Navier-Stokes equations [2, 4]. The patch grid and the Chimera grid approach are available to facilitate the grid generation for complex geometries. In addition, the Chimera method is used for simulations involving moving bodies [5].

2.1 Space and time discretization schemes

Various space discretization schemes are available, among them the 2nd and 4th order central schemes with an artificial

dissipation and Roe and AUSM upwind schemes from 1st to 5th order. Time integration can be made using the explicit Runge-Kutta schemes, or the semi-implicit LU-SGS scheme. Various methods are available to accelerate the convergence to steady state, as for example local time stepping, multigrid and full multigrid, and low Mach number preconditioning. The dual time stepping approach is used for unsteady simulations.

2.2 Turbulence and Transition modelling

NSMB includes a wide variety of well tested turbulence models, among them the Baldwin Lomax algebraic turbulence model [6], the Spalart-Allmaras 1 equation turbulence model [7] and several variants of the k-ω turbulence model, among them the Wilcox model [8] and the Menter Shear Stress model [9]. Transition can either be prescribed on lines or planes, or it is possible to solve 2 additional transport equations [10].

For unsteady simulations different hybrid turbulence models are available as for example the Detached Eddy Simulation (DES) approach and several of its variants [11].

Finally, roughness models have been implemented for the Spalart-Allmaras 1-equation and for the k-ω 2 equation turbulence models [12].

2.3 Chemistry modelling

NSMB was designed for hypersonic applications (re-entry space vehicles), and includes several levels of air chemistry modelling for Air, CO2 and N2. In the original implementation air can be considered as having 5, 7, 11 or 13 chemical species. A large number of non-equilibrium chemistry models have been implemented and for all these models the equilibrium constants for the chemical reactions are computed using the polynomials provided in the references.

Chemical equilibrium can be computed using polynomials (TGAS/VGAS for air [13]), or by calculating the chemical composition for equilibrium using minimization of Gibbs free energy.

Thermochemical non-equilibrium has been implemented using the Landau-Teller equation for the translational-vibrational energy exchange with the relaxation time calculated using the semi empirical Millikan and White [14] formula. All these models are available for inviscid and viscous (both laminar and turbulent) flows.

Transport coefficients are computed using the Blottner [15] or the Gupta Yos [16] model.

More recently NSMB has been coupled to the Mutation^{++} library developed by the Von Karman Institute [17]. Mutation^{++} provides the chemical source terms as well as the transport coefficients for a reacting mixture, and includes models for ablating flows.

2.4 ALE approach

NSMB uses the ALE (Arbitrary Lagrangian Eulerian) approach to simulate flows on moving grids. Three levels of ALE are distinguished:

- Steady ALE - used to simulate flows on non-moving grids, as for example flows in a rotating frame
- Moving grids - used to simulate flows on moving grids, but no grid deformation takes place. This option is for example used for 6 DOF simulations [5].
- Deforming grids. This includes a re-meshing option using either the Volume Spline Interpolation or the Transfinite Interpolation technique.

It is possible to solve the Geometrical Conservation Law on deforming grids.

2.5 Fluid Structure Interaction and Remeshing

NSMB distinguishes 2 levels of fluid structure interaction [18]:

- static deformation of the structure due to aerodynamic loads
- dynamic deformation of the structure due to flutter or limit cycle oscillations

For both levels an external tool is needed to couple fluid and structure grids. Today NSMB is coupled using the fscon tool developed by SMR, which is using the Volume Spline Interpolation method to connect the two grids.

For the static deformation two approaches are available in NSMB:

- Use a linear structural model based on a modal formulation
- Use the B2000++ open source FEM solver [19]

For both approaches the procedure is similar: the aerodynamic forces are computed on the CFD grid and interpolated to the CSM grid. Then the CSM solver (either based on the modal formulation or the B2000++ FEM solver) is used to compute the deformation of the structure. This is translated in to a displacement of surface coordinate points and NSMB uses these displacements to re-compute the CFD grid.

For dynamic fluid structure interaction a linear structural model is employed based on a modal formulation. This is integrated in the NSMB flow solver and no interaction with an external CSM solver is required. During the dual time stepping loop NSMB communicates with the integrated CSM solver by sending the aerodynamic forces and by receivingthe surface displacements. Once the surface displacements are

available the re-meshing procedure is used to recompute the grid.

3. BOW SHOCK ADAPTION PROCEDURE

NSMB includes a bow shock adaption procedure that moves the far-field boundary and clusters the grid points around the shock wave. To permit the use of this procedure it is required that the shock is located in the blocks that have a far-field boundary condition. The initial idea for the shock adaption procedure was to use the re-meshing procedure implemented for fluid structure interaction [18], but this idea appeared to be rather complex to implement. A much simpler procedure is to move the grid points along the mesh lines normal to the far-field boundary.

In the first implementation of the bow shock adaption procedure it was only possible to impose the grid adaption at given time steps of the solver. This procedure had two disadvantages: 1) if the adaption was made too early the shock might leave the computational domain resulting in a divergence of the calculation and 2) if the adaption was made too late computational resources were wasted.

Based on the experience of using the bow shock adaption for a variety of different 2D and 3D cases a methodology was developed that activates the bow shock adaption procedure. The user has only to provide as input the number of times the shock needs to be adapted and how many steps NSMB needs to be made after the last shock adaption.

Note that the shock adaption procedure is independent of the physical modeling (laminar/turbulent, perfect gas, equilibrium, chemical or thermo-chemical non-equilibrium) used in the calculation.

3.1 Procedure to determine the moment of shock adaption

The movement of the bow shock position as well as the convergence of the calculation are used to determine whether the shock needs to be adapted. Every 10 time steps the distance between the far-field boundary and the bow shock location is calculated. Since NSMB is a cell centered solver it is needed to compute the Mach number on the grid lines. Then for each far-field boundary it is determined whether it is an inflow boundary, an outflow boundary, or an inflow boundary with the bow shock leaving the computational domain. In the next step the position of the bow shock on a grid line is determined by moving along the grid line starting at the far-field boundary until a variation in Mach number compared to the freestream Mach number is observed. This variation is set to 0.05 for a freestream Mach number of 3 and lower, 0.10 for a freestream Mach number until 10, and 0.20 for freestream Mach numbers above 10. When a variation of the Mach number is observed linear interpolation is used to calculate the shock position, and the edge length from the far-field boundary until the shock position is computed. These edge lengths are summed up, and divided by the number of points having an inflow boundary to obtain δ, a measure of the movement of the far field boundary. To permit to calculate a measure of convergence the last 4 values are saved. The measure of convergence of the far-field boundary movement is defined as:

$$\varepsilon_s = \left|1 - \frac{\delta^{n-1}}{\delta^n}\right| \qquad (1)$$

With n the time step the far-field boundary movement is calculated. A second parameter is the difference of the average of the last 4 far-field boundary movements. This parameter can be negative, and is also used to detect if the shock movement has changed direction. It often happens that the shock position is oscillating, in particular when the grid is coarse. A counter is used to count the number of times the value of ε_s is below a given threshold. This threshold is set to $5\ 10^{-5}$ for flows with a freestream density $\rho_\infty < 10^{-5}$ and 10^{-4} otherwise. For flows with a low freestream density the shock position converges very slowly since conditions are close to the rarefied flow regime. Note that when the value of ε_s is larger than twice the threshold the counter is reduced.

The final decision to adapt the shock is a mixture of the convergence of the calculation (normalized L2-residue of the continuity equation) and the counter. For values of the L2-residu between $5\ 10^{-2}$ and 10^{-1} the value of the counter should be at least 10 before a shock adaption takes place. For lower values the value of the counter is reduced.

When it is detected that the shock is leaving the computational domain the shock is adapted immediately.

3.2 Re-meshing along grid lines

The actual shock adaption takes places in several steps. In the first step the distance between the far-field boundary and the estimated bow shock position is calculated on each grid line normal to the far-field boundary for each block having a far-field inflow boundary. In the second step a Bezier smoothing procedure is used to smooth these distances to remove spurious oscillations. In the third step the new spacing parameters around the shock (including grid point clustering) and between shock wave and far-field boundary are calculated. In case of a shock adaption due to the shock wave leaving the computational domain the spacing parameters are adjusted to move the far-field boundary away from the shock. In the last step the spacing parameters between the shock position and the block face opposite to the far-field boundary are computed, but with keeping the first spacing untouched. When the new spacing parameters on a given grid line are known it is possible to compute the new coordinates for this block. Once the new grid is known for all blocks the coordinates at block interfaces are exchanged, the metric parameters are re-calculated as well as the distance to the wall for a turbulent calculation.

3.3 Other parameters

After the movement of the far-field boundary it is possible to interpolate the flow solution on the new grid. However, this only works when using the central scheme. When using the upwind scheme the calculation diverges rather quickly when the solution is interpolated on the new grid. It was also observed that for thermo-chemical non-equilibrium calculations it is better to continue the calculation instead of interpolating the solution on the new grid.

When using the automatic shock adaption it is possible to write the parameters that are used to monitor the shock adaptation process to a log file. It is also possible to save the solution just before the shock adaption.

4. RESULTS OF CALCULATIONS

4.1 RAM-C

The RAM-C was a hypersonic flight experiment flown in the 1960's to perform Radio Attenuation Measurements. The vehicle is a spherically blunted cone with a radius of 0.154 m and a length of 1.3m. This case is widely used for CFD code validation, see for example [20]. The 61km altitude case is simulated here, and the freestream conditions are summarized in Table 1.

Mach	ρ_∞ (kg/m^3)	p_∞ (Pa)	T_∞ (K)
23.9	$2.7\ 10^{-4}$	19.7	254

Table 1: Ram-C Freestream conditions at 61 km.

Figure 2 shows the measure of convergence of the far-field boundary movement, ε_s in Eq. (1), together with the L2 density residual during the calculation.

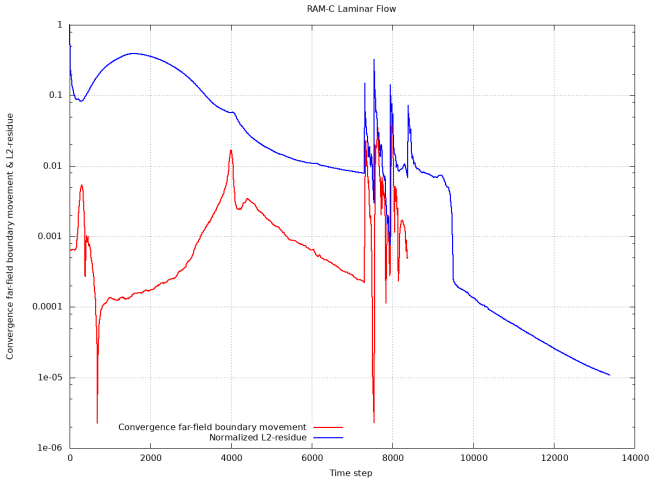

Figure 2: Measure of convergence of the far-field boundary movement and L2-density residual, RAM-C calculation at 61km.

As can be seen the measure of convergence of the far-field boundary movement goes rather quickly to very low values. This is caused by the establishing of the shock at the spherical part of the geometry, but further downstream the shock is still close to the body. Adapting the grid at this moment should be avoided. One can see that ε_s increases gradually until step 4000, after which it then slowly decreases. At the same time the density residual is decreasing and the shock adaption takes place 4 times. After the last adaption the calculation continues and the density residual decreases to 10^{-5} after which the calculation stops.

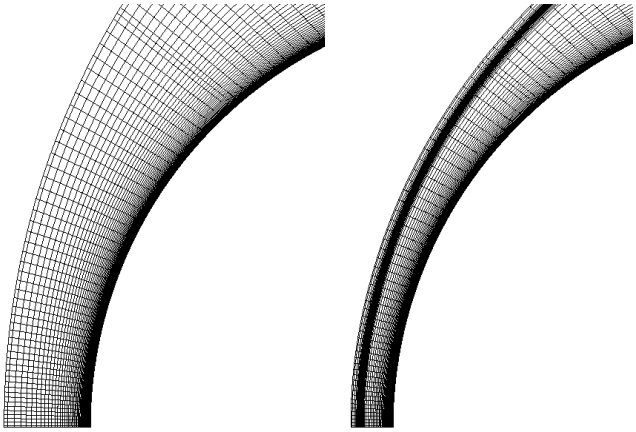

Figure 3: Adapted (right) and un-adapted grid (left) RAM-C at 61 km.

Figure 3 shows the adapted and un-adapted at the nose. One clearly observes the movement of the far-field boundary, and the grid clustering around the shock position.

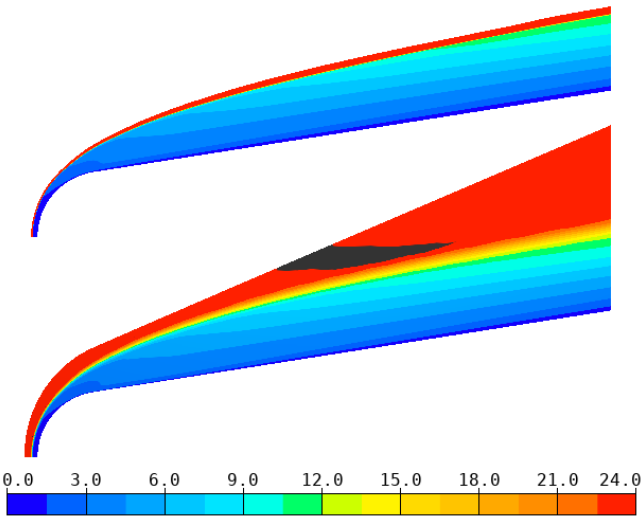

Figure 4: Mach number contours adapted (top) and un-adapted grid (bottom), RAM-C at 61km.

Figure 4 shows the Mach number contours, and one can observe that the spurious oscillations in Mach number on the un-adapted grid have been removed. One can also observe that the shock is much less smeared out when using shock adaption.

4.2 EDL system

A large number of CFD simulations were made for an Entry Descent and Landing system for the planet Mars [21]. A single grid was used for the hypersonic flow cases, ranging from Mach=5 until Mach=30, for different Angles of Attack (AoA) between 0º and 15º. The starting grid is shown in Figure 5 together with the 5 times adapted grid for the Mach=23, AoA=15º calculation. The flow conditions for the Mach=23 calculations are summarized in Table 2. The calculations were made for a CO_2 atmosphere considering 9 chemical species and 61 chemical reactions.

Mach	ρ_∞ (kg/m^3)	p_∞ (Pa)	T_∞ (K)
23	$1.69196\ 10^{-4}$	4.8308	149.434

Table 2: Freestream conditions EDL calculations at Mach=23.

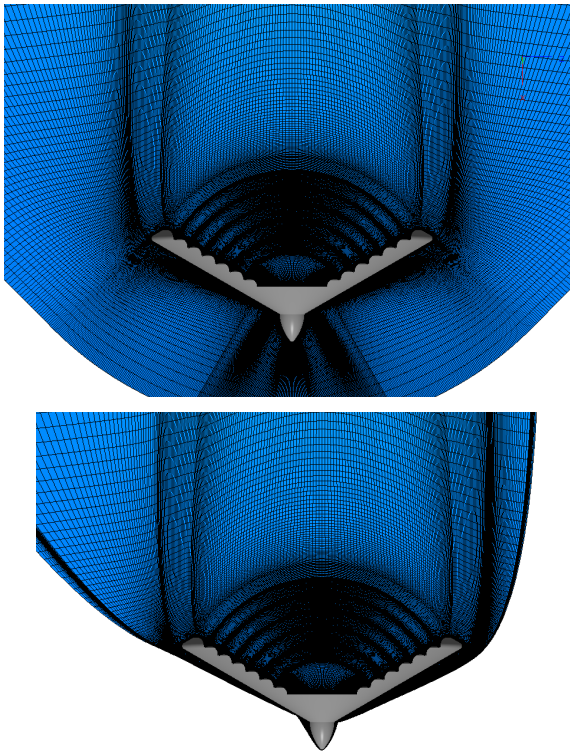

Figure 5: Starting grid (top) and 5 times adapted grid EDL system, Mach=23, AoA=15º.

The large movement of the far-field boundary, and the clustering of the grid lines near the bow shock wave can be clearly seen in Figure 5.

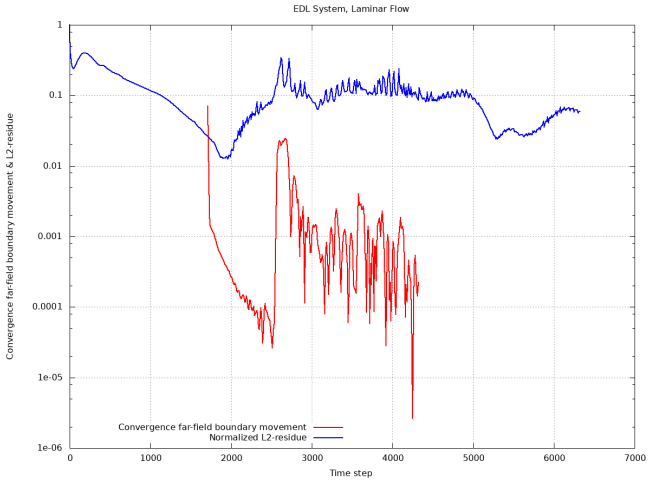

Figure 6: Measure of convergence of the far-field boundary movement and L2-density residual, EDL calculation at Mach=23, AoA=15º.

Figure 6 shows the convergence of the far-field boundary movement as well as the L2-density residual for this calculation. The first adaption takes place after 2500 steps because the far-field boundary movement has sufficiently converged, despite the fact that the L2-residual is increasing. The 2nd adaption takes place at 3550 steps, followed by adaptions at 3810, 4070 and 4320 steps. The fact that the L2-residual is increasing is due to an unsteady zone on the leeward side of the configuration where the relatively high angle of attack creates a large separation zone.

Figure 7 shows a zoom of the junction inflatable part – penetrator system for the un-adapted and adapted grid for the Mach=23, AoA=15º calculation. The bow shock is much better captured on the adapted grid leading to a sharper shock-shock interaction, and a better resolution of the maximum heat flux on the penetrator. This maximum heat flux is due to the thin boundary layer caused by the shock-shock interaction.

4.3 ATD3 Shock-shock interaction case

In the frame of the ATD3 (AeroThermoDynamics for Design for Demise) workshop the shock-shock interaction case was computed using automatic shock adaption. The freestream conditions are summarized in Table 3.

Mach	p_∞ (Pa)	T_∞ (K)	Re (1/m)
7	125.61	55.56	$2.2\ 10^6$

Table 3: Freestream conditions shock-shock interaction problem.

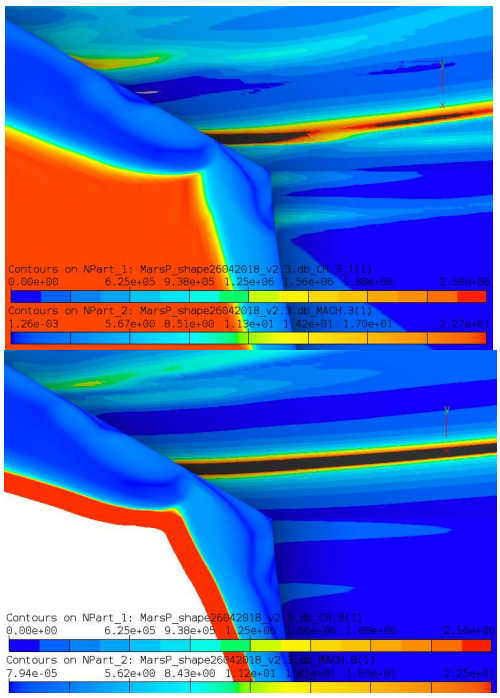

Figure 7: Mach number contours (symmetry plane) and heat flux (on the body) at the junction inflatable part and penetrator, Mach=23, AoA=15.

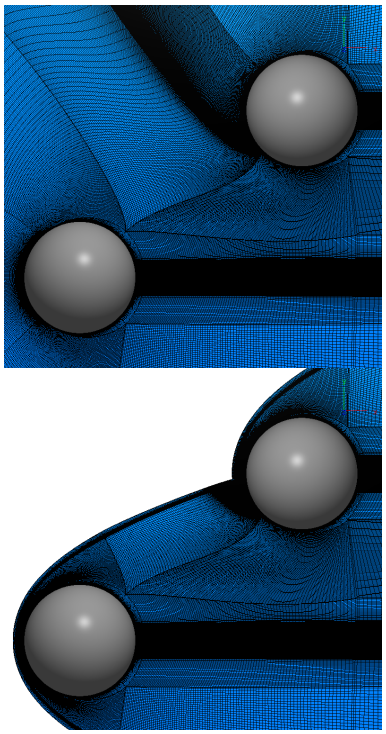

Figure 8: Shock-shock interaction problem Case B. Top before shock adaption, bottom adapted grid.

The flow was treated as a perfect gas, and both laminar and turbulent calculations were made. Two cases were considered, case A with a sting on both spheres, and case B without the stings. Figure 8 shows the un-adapted and adapted grid for case B. For this calculation the grid was adapted 10 times. Figure 9 shows the Mach numbers in the symmetry plane for the laminar calculations for Case A and Case B, and one can clearly observe the influence of the sting on the flow.

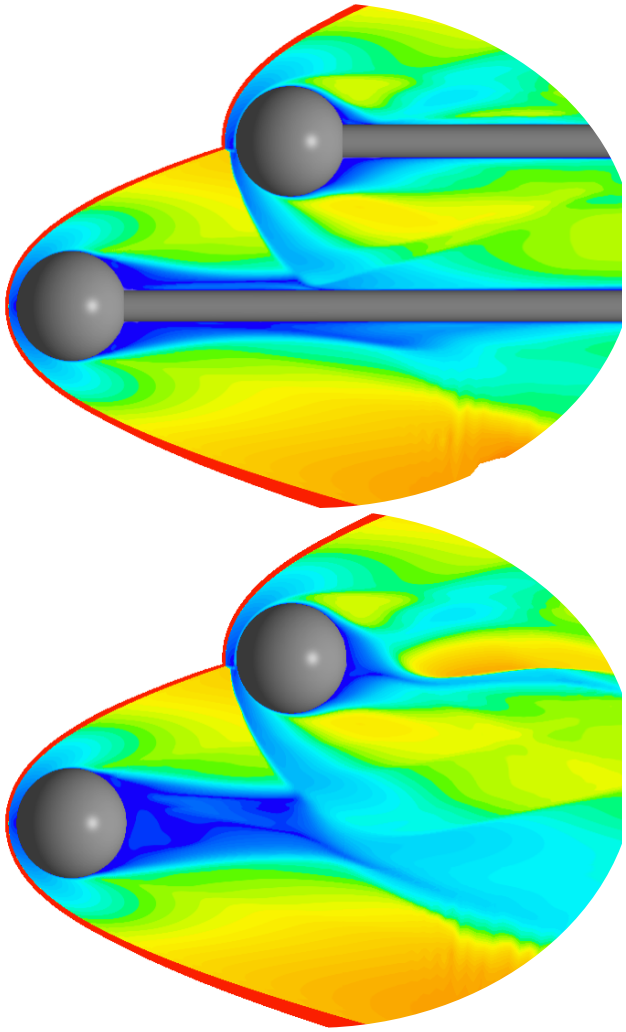

Figure 9: Shock-shock interaction case, laminar flow.

Figure 10 shows the wall heat flux on the top sphere for the laminar calculation without sting. Due to the shock-shock interaction the boundary layer is thin, leading to a zone with high values of the heat flux. The shock adaption procedure results in a better capturing of the shock-shock interaction, and in a more precise approximation of the zone of high heat fluxes.

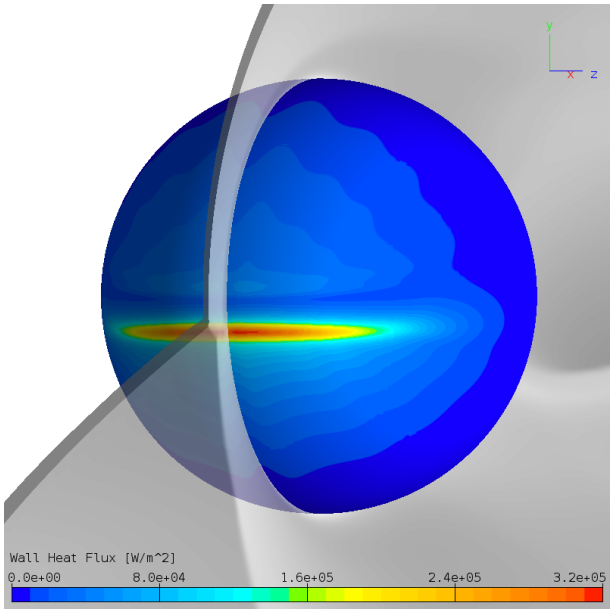

Figure 10: Wall heat flux on the top sphere, laminar flow without sting.

5. CONCLUSIONS

An automatic bow shock adaption procedure was implemented in the NSMB CFD solver. This procedure automatically adapts the far-field boundary to the bow shock wave, and clusters grid points around this shock wave to improve the shock resolution. The implemented method is independent of the physical modeling, can be used from low supersonic to hypersonic Mach numbers.

Using bow shock adaption leads to improved resolutions of the pressure and force coefficients and of the heat fluxes, in particular for capsule type geometries.

The implemented procedure removes the tedious effort to adapt the grid for each flow case to be simulated. Today a well-designed grid can be used for many flow cases to be simulated, leading to considerable savings in manpower needed for grid generation.

10. REFERENCES

[1] E.H. Hirschel, *Basics of Aerothermodynamics*, Springer Verlag, Berlin Heidelberg, 2005.

[2] J.B. Vos, A.W. Rizzi, A. Corjon, E. Chaput and E. Soinne Recent Advances in Aerodynamics inside the NSMB (Navier Stokes Multi Block) Consortium, Invited Talk AIAA 36th Aerospace Sciences Meeting, January 1998.

[3] J.F. Pallegoix and J. Collinet, "Atmospheric Re-entry Demonstrator: Post Flight Analysis, Flight Rebuilding with CFD control.", 2nd International Symposium – Atmospheric Reentry Vehicles and Systems, Arcachon, March 2001.

[4] Y. Hoarau, D. Pena, J.B. Vos, D. Charbonnier, A. Gehri, M. Braza, T. Deloze, E. Laurendeau, Recent Developments of the Navier Stokes Multi Block (NSMB) CFD solver. AIAA Scitech Conference, 2016-2056.

[5] D. Charbonnier, J. B. Vos, E. Clopeau, L. Ferracina, L. Marraffa, Marcopolo-R ERC Dynamic Characterization: Computational Campaign, ESA 8th Aerothermodynamics Conference, March 2015.

[6] B.S. Baldwin and H. Lomax, Thin Layer Approximation and Algebraic Model for Separated Turbulent Flows, AIAA-paper 78-257, 1978.

[7] P.R. Spalart and S.R. Allmaras, A One-Equation Turbulence Model for Aerodynamic Flows, AIAA Paper 92-0439, Jan. 1992.

[8] D.C. Wilcox, Turbulence Modeling for CFD, DCW Industries, Inc. La Casada, California, 1993.

[9] F.R. Menter, A Zonal Two Equation k-w Turbulence Models for Aerodynamic Flows, AIAA paper, vol. 93-2906, 1993.

[10] R. Langtry and F.R. Menter, Correlation-based transition modeling for unstructured parallized computational fluid dynamic codes. *AIAA Journal*, Vol. 47, pp. 2894-2907, 2009.

[11] P.R. Spalart, Detached Eddy Simulation, *Annual Review of Fluid Mechanics*, Vol. 41, pp. 181-202, 2009.

[12] J.B. Vos, A. Bourgoing, B. Rey, J. Soler, Earth Re-entry Capsule CFD simulations, *International Journal of Aerodynamics*, Vol. 5, No.1, 2015.

[13] S. Srinivasan, J.C. Tannehill, and K.J. Weilmunster, Simplified Curve Fits for the Thermodynamic Properties of Equilibrium Air, NASA Reference Publication 1181, August 1987.

[14] R.C. Millikan and D.R. White, Systematics of vibrational relaxation *J. of Chemical Physics* 39 (12), 1963.

[15] F.G. Blottner, M. Johnson, and M. Ellis, Chemically Reacting Viscous Flow Program for Multi Component Gas Mixture, Sandia Laboratories, SC-RR-70-754, 1970.

[16] R.N. Gupta, J.M. Yos, R.A. Thompson and K-P Lee, A Review of Reaction Rates and Thermodynamic and Transport Properties for an 11-Species Air Model for Chemical and Thermal Nonequilibrium Calculations to 30 000K, NASA Reference Publication 1232, 1990.

[17] J.B. Scoggins and T.E. Magnin, Development of Mutation^{++}: MUlticomponent Thermodynamic And Transport properties for IONized gases library in C^{++}, AIAA Paper 2014-2966, 2014.

[18] J.B. Vos, D. Charbonnier, T. Ludwig, A. Gehri, P. Stephani, Recent Developments on Fluid Structure Interaction in the Navier Stokes Multi Block (NSMB) CFD solver, AIAA Aviation Conference, 2017-4458.

[19] http://www.smr.ch/products/b2000/

[20] E. Farber and I.D. Boyd, Numerical Prediction of Hypersonic Flowfields Including Effects of Electron Translational Non-equilibrium, *Journal of Thermophysics and Heat Transfer*, Vol. 27, No. 4 2013.

[21] D. Chaillot, H.U. Quaranta, A. Santerre, G. Pinaud, J. Vos, L. Ferracina, Aerothermodynamics assessment of an entry descent and landing system for a penetrator mission on Mars, FAR2019, 2019.